POLITECNICO DI TORINO
Repository ISTITUZIONALE

EnvShip: A Unified Framework for Context-Aware and Cross-Region Vessel Trajectory Forecasting

Original
EnvShip: A Unified Framework for Context-Aware and Cross-Region Vessel Trajectory Forecasting / Ma, K., Han, Q., Yao, J., Song, C., Wang, H., Wu, C., Chiasserini, C.F.. - (2027). (ACM KDD 2027 San Jose (USA)).

Availability:
This version is available at: 11583/3017727 since: 2026-11-10T08:49:18Z

Publisher:
ACM

Published
DOI:

Terms of use:

This article is made available under terms and conditions as specified in the corresponding bibliographic description in the repository

Publisher copyright
IEEE postprint/Author's Accepted Manuscript

©2027 IEEE. Personal use of this material is permitted. Permission from IEEE must be obtained for all other uses, in any current or future media, including reprinting/republishing this material for advertising or promotional purposes, creating new collecting works, for resale or lists, or reuse of any copyrighted component of this work in other works.

(Article begins on next page)

10 November 2026

EnvShip: A Unified Framework for Context-Aware and Cross-Region Vessel Trajectory Forecasting

Kun Ma
Harbin Engineering University
Harbin, China
Politecnico di Torino
Turin, Italy

Qilong Han
Harbin Engineering University
Harbin, China

Jingzheng Yao
Harbin Engineering University
Harbin, China

Chengjing Song
Harbin Engineering University
Harbin, China

Hao Wang
Harbin Engineering University
Harbin, China

Changmao Wu
Chinese Academy of Sciences
Beijing, China

Carla Fabiana Chiasserini
Politecnico di Torino
Turin, Italy

Abstract

Accurate vessel trajectory forecasting is essential for maritime situational awareness, navigation safety, traffic management, and autonomous navigation. Public Automatic Identification System (AIS) archives have enabled extensive research in this area, yet results remain difficult to compare because existing studies use incompatible preprocessing pipelines, forecasting horizons, data splits, coordinate systems, contextual inputs, and evaluation settings. We present EnvShip, a unified multi-region framework for context-aware and cross-region vessel trajectory forecasting. EnvShip applies a fixed and reproducible pipeline to public AIS data from Denmark, the United States, Greece, and Norway, and defines two standardized forecasting tracks spanning short- and long-horizon settings. From large-scale processed data, we curate 330,000 short-term and 106,857 long-horizon samples through strict motion screening, vessel-category and difficulty stratification, redundancy control, and vessel-disjoint splits. Each sample is aligned with environmental and neighboring-vessel context, together with weather and sea-state variables where available. We evaluate representative methods under in-domain and cross-region protocols, with analyses across prediction difficulty, scene type, and random seeds. Results show that environmental context provides the largest gains in coastline-constrained scenes, whereas neighboring-vessel context primarily benefits interaction-rich cases. Multi-region training improves generalization in most settings but introduces negative transfer for some source combinations. EnvShip provides a common and reproducible testbed for vessel trajectory forecasting.

CCS Concepts

• **Computing methodologies** → **Tracking**; • **Information systems** → *Data mining*.

Keywords

Vessel trajectory prediction; AIS dataset; context-aware maritime benchmark; cross-domain transfer

1 Introduction

Maritime transport carries more than 80% of international trade in goods by volume, making safe and efficient vessel operations important to global supply chains [45]. A key capability is to predict how vessels will move in the near future. Vessel trajectory forecasting supports route monitoring, collision-risk assessment, traffic management, anomaly detection, port operations, and autonomous navigation.

The Automatic Identification System (AIS) continuously reports vessel positions and motion states, and public AIS archives have enabled extensive research on data-driven vessel forecasting [5, 19, 21, 30, 36, 44, 53]. However, results from different studies are often not directly comparable. Existing works commonly use different rules for data cleaning, trajectory segmentation, interpolation, and resampling. They also differ in observation and prediction horizons, coordinate systems, data splits, contextual inputs, and evaluation settings [8, 51–53]. Consequently, an apparent improvement may reflect differences in data or task construction rather than the forecasting model itself.

Most public AIS resources are trajectory-centric and do not provide environmental or neighboring-vessel information aligned with each forecasting sample, although coastlines, navigable waterways, port geometry, and surrounding traffic can constrain vessel motion [11, 20, 37, 39]. Moreover, most resources cover a single country, port, or waterway [10, 37, 42, 43]. This makes it difficult to determine whether a conclusion obtained in one navigation environment remains valid in another. To address these limitations, we present **EnvShip**, a unified multi-region framework for context-aware and cross-region vessel trajectory forecasting. EnvShip processes four public AIS sources through a fixed and reproducible pipeline: the Danish Maritime Authority archive, the NOAA MarineCadastre archive for United States waters, the Piraeus dataset from Greece, and the Kystverket feed for Norwegian coastal waters. Together, these sources cover open-water transit, coastal navigation, port operations, ferry traffic, and constrained waterways.

EnvShip defines two standardized tracks at 20-s intervals: Track A uses 10 min of observation and up to 10 min of prediction, whereas Track B uses 30 min of observation and up to 60 min of prediction. From large-scale regional cores, we curate 330,000 short-term and 106,857 long-horizon samples using motion screening, vessel-category and difficulty stratification, redundancy control, and vessel-disjoint splits. Each forecasting sample is aligned with environmental geometry, neighboring-vessel

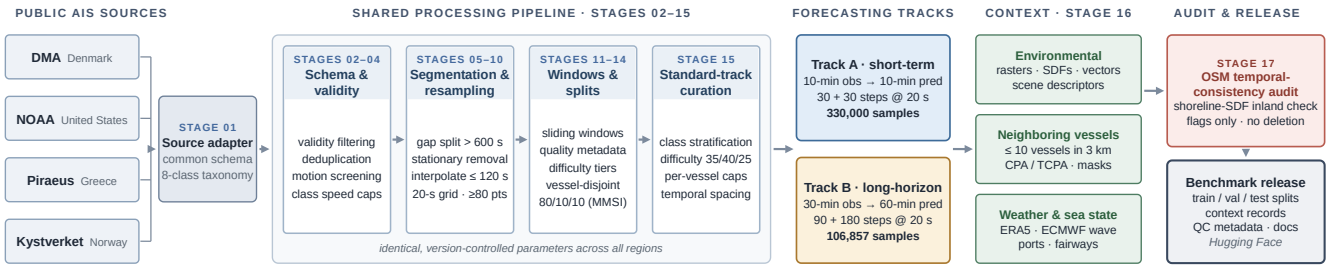


Figure 1: EnvShip construction pipeline. Four public AIS sources are processed through a shared pipeline to produce two forecasting tracks with aligned context and quality-control metadata.

interactions, and weather and sea-state variables where available. Figure 1 summarizes the complete construction and release pipeline. The release also includes sample-level quality metadata and an OpenStreetMap temporal-consistency flag for map changes that can make historical trajectories appear inland [14, 33].

We evaluate representative methods from four families: physics-based methods, classical machine-learning methods, trajectory-only deep models, and context-aware deep models. The evaluation covers both forecasting tracks and all four regions. Beyond aggregate in-domain results, we report performance by prediction difficulty, scene type, and neighboring-vessel density. We also conduct a multi-seed stability analysis, long-horizon evaluation, and combined and leave-one-source-out (LOSO) cross-region experiments.

The evaluation addresses three questions: (1) when contextual information improves vessel forecasting, (2) whether conclusions obtained in one region generalize to other regions, and (3) how stable model performance remains across horizons and random seeds. The results show that environmental context provides the largest gains when coastline geometry constrains vessel motion, whereas social context mainly benefits interaction-rich samples. Multi-region training generally improves robustness and helps data-scarce regions, but combining substantially different navigation regimes can introduce negative transfer. Some context-aware models are also more sensitive to random initialization than trajectory-only baselines, highlighting the importance of multi-seed evaluation.

The main contributions of this work are thus as follows:

- **A unified multi-region and multi-horizon framework.** EnvShip processes public AIS data from four maritime regions through one reproducible pipeline and defines two multi-horizon forecasting tracks with vessel-disjoint splits, thereby preventing cross-split leakage from overlapping sliding windows of the same vessel.
- **Sample-aligned context with quality control.** Each sample is aligned with environmental, neighboring-vessel, weather, and sea-state information, along with sample-level quality metadata and an OpenStreetMap temporal-consistency flag.
- **A comprehensive forecasting evaluation.** We evaluate representative methods under difficulty- and scene-stratified, multi-seed, in-domain, multi-horizon, and cross-region settings. Experimental results reveal when contextual information and multi-region training benefit or degrade forecasting performance.

2 Related Work

Public AIS resources and forecasting protocols. Public AIS data are available as raw national archives, processed regional corpora, and task-specific datasets. The Danish Maritime Authority archive [9] and NOAA AccessAIS [25, 31] provide large-scale point-level AIS records from which users must construct trajectories and forecasting tasks. Processed regional resources include the Piraeus dataset [43], the Ushant corpus [10], and the Brest datasets [37, 50]. The DTU dataset, in contrast, was developed primarily for abnormal-behavior detection rather than trajectory forecasting [42]. Piraeus and Brest also provide vessel, geographic, or environmental information, but these data are distributed at the dataset level rather than aligned with fixed forecasting samples.

Several forecasting studies define more detailed experimental settings. TrAISformer [30] uses a processed Danish AIS subset with a study-specific temporal split and a long-horizon forecasting task, while MSTFormer [36] evaluates multiple forecasting settings constructed from NOAA AIS data. These datasets and protocols are useful for evaluating their associated methods, but remain tied to individual studies. As summarized in Table 1, the representative prior resources either require user-defined task construction or provide study-specific forecasting settings without sample-aligned external context. None combines fixed multi-horizon tasks, vessel-disjoint splits, sample-aligned maritime context, and cross-region evaluation under one common protocol.

AIS-based vessel trajectory forecasting. Vessel trajectory forecasting methods range from kinematic and classical machine-learning approaches to recurrent, Transformer-based, and probabilistic models. Recurrent and sequence-to-sequence methods learn temporal motion patterns from historical AIS observations [5, 21, 41, 48]. TrAISformer and MSTFormer use Transformer architectures to capture longer-range temporal dependencies [30, 36]. Other studies incorporate geographic constraints, neighboring-vessel interactions, regional motion patterns, or predictive uncertainty [11, 20, 23, 24, 26, 28, 39].

Despite these advances, most methods are evaluated on independently processed regional subsets. Differences in data cleaning, trajectory construction, forecasting tasks, and evaluation splits therefore remain difficult to separate from differences in model design. EnvShip is method-agnostic: it fixes these factors and provides a common basis for comparing existing and future forecasting methods under consistent conditions.

Table 1: Comparison of representative public AIS resources and study-associated datasets for vessel trajectory forecasting

Resource	Coverage	Release / primary use	Reported scale	Forecast protocol	Evaluation split	Context support
Raw national AIS archives						
DMA Historical AIS [9]	Danish waters	Raw national AIS archive	Multi-year monthly CSV/ZIP files	User-defined	User-defined	AIS positions and motion states, vessel identifiers, type, dimensions, and navigational status; no aligned external context
NOAA AccessAIS / MarineCadastre [25, 31]	U.S. coastal and inland waters	AIS archive and data-query service	National-scale, multi-year terrestrial AIS records	User-defined	User-defined	AIS positions and motion states, vessel identifiers, type, dimensions, and navigational status; no aligned external context
Processed regional AIS resources						
Piraeus AIS dataset [43]	Piraeus and Saronic Gulf, Greece	Regional maritime mobility dataset	244M+ records over 2.5+ years	User-defined	User-defined	Vessel, geographic-area, and meteorological information provided as dataset-level tables
Ushant AIS dataset [10]	Ushant TSS, France	Processed trajectory corpus	18,603 trajectories and 7M+ observations over 6 months	User-defined	User-defined	Trajectory sequences and vessel-category metadata; no aligned environmental or interaction context
Brest integrated dataset [37]	French Atlantic, English Channel, and Bay of Biscay	Integrated maritime intelligence dataset	6 months of multi-source maritime data	User-defined	User-defined	Vessel and navigation data with ports, coastlines, maritime zones, ocean conditions, and weather at dataset level
Forecasting-oriented processed datasets						
TrAISformer processed set [30]	Danish Straits	Study-associated long-horizon forecasting data	Jan.–Mar. 2019; approximately 712M raw AIS messages	3-h observation to up to 15-h prediction; 10-min sampling	Study-defined temporal split	Latitude, longitude, SOG, COG, timestamp, and vessel identifier sequences; no external context
MSTFormer datasets [36]	Gulf of Mexico	Study-associated forecasting datasets	43,000–172,100 windows across four settings	Four study-defined observation–prediction settings; 1- or 3-min sampling	Study-defined 70/10/20 split	AIS motion attributes and derived speed- and course-change features; no external context
EnvShip (ours)	**Denmark, U.S., Greece, and Norway**	**Unified forecasting benchmark and framework**	**9.5M regional-core windows, 330,000 short-term and 106,857 long-horizon benchmark samples**	**10-min observation, up to 10-min prediction; 30-min observation, up to 60-min prediction; 20-s sampling**	**Fixed vessel-disjoint train/validation/test splits**	**Dynamic and static AIS attributes; environmental rasters, SDFs, shorelines, and scene descriptors; neighboring-vessel histories with CPA/TCPA; weather and sea-state variables; and quality metadata aligned with each sample**

Context-aware trajectory benchmarks in neighboring domains. Pedestrian forecasting has long relied on shared evaluation resources such as ETH and UCY [18, 34] and the Stanford Drone Dataset [38]. These datasets have supported the development and comparison of models for social interaction and multimodal motion, including Social-LSTM, Social-GAN, and Social-STGCNN [1, 13, 27]. Interaction-rich multi-agent forecasting has also been studied using NBA player-tracking data [15].

In autonomous driving, Argoverse and nuScenes combine agent trajectories with map and scene information [4, 6], supporting context-aware models such as Trajectron++, Scene Transformer, AgentFormer, and HiVT [29, 40, 49, 54]. Maritime forecasting has likewise begun to incorporate environmental constraints and vessel interactions [11, 20, 26, 28], but existing studies still rely largely on study-specific data construction and evaluation. EnvShip extends the shared-benchmark paradigm to maritime forecasting by unifying fixed multi-horizon tasks, vessel-disjoint splits, sample-aligned environmental and neighboring-vessel context, and cross-region evaluation within a reproducible pipeline. This controlled design isolates context utility and geographic transfer from differences in task construction.

3 The EnvShip Benchmark

This section describes the task definition, shared construction pipeline, track curation, and context alignment. Complete schemas, directory layouts, and field definitions are provided with the public dataset release.

3.1 Data Sources and Forecasting Protocol

EnvShip is constructed from four public AIS sources: the Danish Maritime Authority archive [9], NOAA MarineCadastre [25], the Piraeus dataset [43], and the Norwegian Kystverket feed [32]. Table 2 summarizes the source periods, anchor extents, unique vessel counts, candidate windows, and released benchmark samples. Candidate windows are quality-filtered forecasting windows generated before standard-track curation. Vessel counts denote unique MMSIs within each source, and the total is the sum across the four sources.

Track A and Track B are generated from the same regional trajectory cores but impose different duration requirements and forecasting windows. All trajectories are sampled at 20-second intervals and represented in a target-vessel-centered metric frame. Geographic coordinates are first projected into a local east–north coordinate system. The final observed position, referred to as the *anchor*, is translated to the origin, and the coordinate frame is rotated according to the final observed heading. Track A contains $T_h = 30$ observed and $T_f = 30$ future positions, corresponding to 10 minutes of observation and 10 minutes of prediction. Track B contains $T_h = 90$ observed and $T_f = 180$ future positions, corresponding to 30 minutes of observation and 60 minutes of prediction. Let

$$\mathbf{X} = \{(x_t, y_t)\}_{t=1}^{T_h}, \qquad \mathbf{Y} = \{(x_t, y_t)\}_{t=T_h+1}^{T_h+T_f}.$$

The task is to predict the future trajectory $\mathbf{Y}$ from the observed $\mathbf{X}$, optionally conditioned on the sample-aligned contextual data.

3.2 Shared Construction Pipeline

Only the source adapter is source-specific, and all downstream stages follow the same processing pipeline, with shared parameters defined in version-controlled configuration files.

Normalization and filtering. Records are mapped to a common schema containing MMSI, UTC timestamp, position, speed over ground (SOG), course over ground (COG), heading, navigation status, and available static vessel attributes. Source-specific vessel types are mapped to a shared eight-category taxonomy. Records with invalid identifiers, timestamps, positions, or speeds are removed, and source-specific AIS sentinel values are treated as missing. Duplicate vessel–timestamp reports are resolved by retaining the record with the most complete fields. Motion screening applies a global speed limit of 55 kn and category-specific limits of 35 kn for cargo vessels and tankers, 45 kn for passenger vessels and ferries, 25 kn for fishing vessels, and 20 kn for tug and service vessels.

Table 2: Per-region coverage and released benchmark size. Anchor extents and vessel counts are computed from the released samples. "Filtered" denotes samples passing the OpenStreetMap temporal-consistency audit in Section 3.5

Source / region	Time span	Anchor extent	Vessels	Candidate windows	Track A: 10/10 min		Track B: 30/60 min	
					Train / Val / Test	Full / filtered (ret.)	Train / Val / Test	Full / filtered (ret.)
DMA / Denmark	2025-09-01–2025-09-30	52.7–59.9°N; 2.1–19.7°E	4,014	5.48 M	120,000 / 15,000 / 15,000	150,000 / 148,883 (99.26%)	46,744 / 5,414 / 6,000	58,158 / 57,713 (99.24%)
NOAA / United States	2025-03-01–2025-03-31	13.7–49.5°N; 159.1°W–144.3°E	3,379	3.55 M	48,000 / 6,000 / 6,000	60,000 / 59,580 (99.30%)	35,893 / 4,725 / 4,148	44,766 / 37,612 (84.02%)
Piraeus / Greece	2019-01-01–2019-12-26	37.7–38.0°N; 23.1–23.7°E	1,775	158 K	48,000 / 6,000 / 6,000	60,000 / 59,770 (99.62%)	628 / 394 / 132	1,154 / 1,154 (100.00%)
Kystverket / Norway	2025-08-01–2025-09-30	57.5–60.5°N; 4.0–11.9°E	687	289 K	48,000 / 6,000 / 6,000	60,000 / 58,083 (96.81%)	2,441 / 117 / 221	2,779 / 2,712 (97.59%)
Total (4 regions)	–	–	**9,855**	**9.48 M**	**264,000 / 33,000 / 33,000**	**330,000 / 326,316 (98.88%)**	**85,706 / 10,650 / 10,501**	**106,857 / 99,191 (92.83%)**

Segmentation and resampling. Records are ordered by vessel and divided at temporal gaps exceeding 600 s, non-monotonic timestamps, or physically implausible implied motion. Segments dominated by anchored, moored, or near-stationary behavior are excluded. Gaps of up to 120 s are interpolated in a local metric frame, with circular interpolation applied to COG and heading. Longer gaps are not bridged. Valid segments are resampled on a common 20-second UTC grid, screened again for geometric inconsistencies, and required to contain at least 80 points.

Window construction and quality metadata. Sliding windows are extracted under the two forecasting protocols. Each sample is accompanied by quality metadata describing its interpolation ratio, displacement, path efficiency, speed variation, and temporal continuity, together with an environmental scene label. Motivated by the challenging-scenario curation of Argoverse 2 [47] and the scenario-stratified evaluation of CRITERIA [7], we introduce a maritime-specific trajectory difficulty score based on the mean and peak turning behavior over the complete observed-and-future window. Larger and more frequent turns indicate greater forecasting difficulty. The score is used only for sample curation and stratified evaluation, not as a model input:

$$D_i = \bar{\theta}_i^{\text{hist}} + \bar{\theta}_i^{\text{fut}} + 0.5\left(\theta_i^{\text{max,hist}} + \theta_i^{\text{max,fut}}\right) + \theta_i^{\text{bridge}} + e_i^{\text{cog}}, \qquad (1)$$

where $\bar{\theta}$ and $\theta^{\max}$ denote the mean and maximum absolute stepwise turning angles over the observed or future trajectory. The term θ^{bridge} measures the turn across the observation–prediction boundary, and e^{cog} is the mean absolute difference between reported COG and motion-derived heading. All angular differences are circularly wrapped and expressed in degrees. Samples are assigned to easy ($D_i < 5$), medium ($5 \le D_i < 12$), and hard ($D_i \ge 12$) tiers. Because this score uses the future trajectory, it is used only for sample curation and stratified evaluation, not as a forecasting input.

Samples are assigned to the training, validation, and test sets at an 80/10/10 ratio using a deterministic hash of the MMSI. The resulting splits are vessel-disjoint, preventing windows from the same vessel from appearing in multiple splits.

3.3 Standard-Track Curation

The standard tracks are curated from the regional core sets through vessel-class stratification, difficulty balancing, quality-based ranking, and redundancy control. Vessel-class proportions are controlled at the benchmark level rather than enforced independently for each region, allowing the curated tracks to retain regional differences in fleet composition and operating patterns. Samples are balanced across easy, medium, and hard cases at a ratio of 35/40/25. As shown in Fig. 2, the four regions remain distinct in their vessel-class composition, historical speed distribution, and 10-minute future displacement. To reduce near-duplicate motion windows, selections are capped per vessel and continuous segment, with a minimum temporal separation between windows from the same segment. The training split contains at most 55 windows per vessel and 12 per segment; for validation and test, the corresponding caps are 70 and 20. Track A therefore contains 330,000 samples: 150,000 from DMA and 60,000 from each of the other three sources.

Figure 3 illustrates the geographic coverage of the DMA Track A anchors. The training, validation, and test splits broadly cover the same principal operating areas, while the density map highlights the concentration of samples along major traffic corridors and other high-traffic areas. Because split assignment is vessel-disjoint, this geographic overlap does not introduce vessel-level leakage.

3.4 Context Packages

A stable sample identifier links each forecasting window to its context records while preserving the trajectory target and split assignment.

Environmental context. For both tracks, OpenStreetMap coastlines, waterways, piers, breakwaters, quays, and port-related features are projected into the target-centered local frame and cropped once at the anchor to an axis-aligned 10 km × 10 km window (±5 km per axis). The package includes a six-channel 128×128 raster encoding land, water, navigable water, natural and man-made boundaries, and barriers; two signed-distance fields, d_{shore} and d_{nav}; clipped vector polylines; and a 14-dimensional scene descriptor summarizing scene type, distance, area ratio, boundary density, and context quality.

Neighboring-vessel context. For each target sample, up to ten nearest vessels within a 3 km radius are selected according to their distance at the anchor time. The released context records contain target-relative neighbor trajectories, relative velocities, pairwise distances, and validity masks that indicate the availability of neighboring-vessel states. They also include the Closest Point of Approach (CPA) and Time to Closest Point of Approach (TCPA) for each target–neighbor pair. Both quantities are computed exclusively from motion states available at the anchor time and therefore do not use any information from the prediction interval. Figure 4 reports the regional distributions of the minimum CPA and absolute TCPA in Track A, together with the proportion of samples containing at least one neighboring-vessel interaction.

Weather, sea-state, and traffic attributes. Each sample includes six weather variables from the ERA5 reanalysis dataset, four wave and sea-state variables from the European Centre for Medium-Range Weather Forecasts (ECMWF) Wave Model, information about

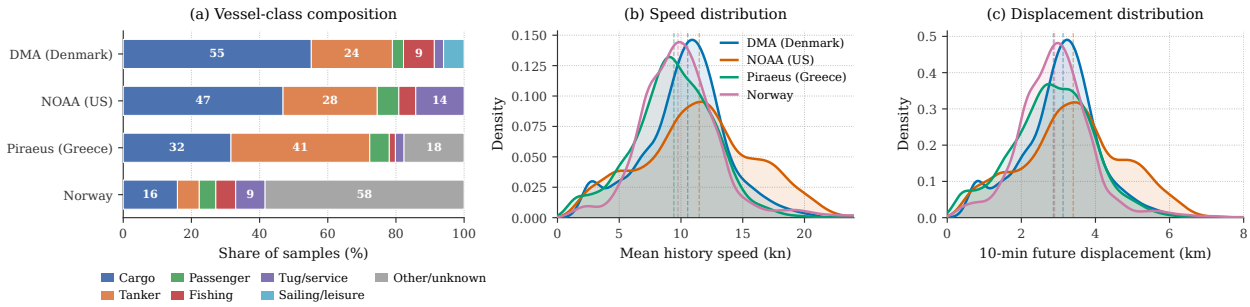


Figure 2: Regional statistics for Track A (330,000 samples). Dashed lines in (b) and (c) denote regional medians.

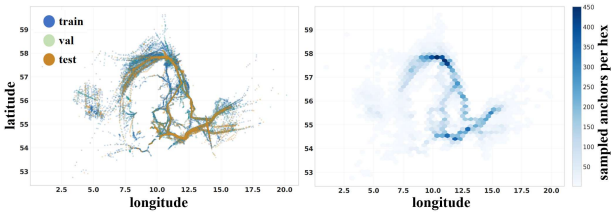


Figure 3: Geographic coverage of DMA Track A anchors. Left: anchor locations in the training, validation, and test splits. Right: hexagonal-bin density of all released anchors.

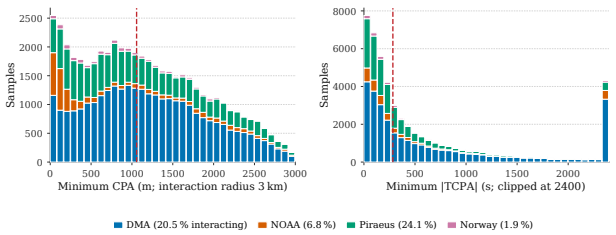


Figure 4: Neighboring-vessel interaction statistics for Track A. Regional distributions of minimum CPA and absolute TCPA; legend indicates the proportion of interacting samples.

the nearest port, and three indicators describing nearby fairways and traffic-separation schemes derived from OpenStreetMap. If a data source does not cover a particular sample, the corresponding attributes are marked as unavailable rather than estimated or imputed.

3.5 OpenStreetMap Temporal-Consistency Audit

OpenStreetMap [14, 33] changes over time. Coastal infrastructure added after the AIS observation period, including reclaimed land, piers, and breakwaters, may cause historically valid vessel trajectories to appear inland when evaluated against a later map snapshot.

The audit projects each trajectory point onto its shoreline signed-distance field and records maximum inland penetration, the number of inland points, and the longest consecutive inland sequence. A sample passes the recommended filter when its inland depth does not exceed 30 m and fewer than three consecutive points are inland.

No sample is deleted. The audit flags and diagnostic values are included in the release, allowing users to select either the complete or recommended subset. The filter retains 326,316 of the 330,000 Track A samples and 99,191 of the 106,857 Track B samples.

Because the Piraeus AIS observations were collected in 2019, its environmental context is additionally constructed using a pinned OpenStreetMap snapshot dated 2020-01-01. The corresponding consistency audit uses the same snapshot. Unless stated otherwise, all experiments use the recommended temporally consistent subset.

4 Evaluation Setup

4.1 Tasks and Metrics

EnvShip evaluates physics-based, classical machine-learning, trajectory-only deep, and context-aware models under a common forecasting protocol. The learned context-aware comparison uses four matched input configurations: trajectory-only, neighboring-vessel-aware, environment-aware, and joint-context forecasting. Prediction targets, vessel-disjoint splits, coordinate frames, and evaluation metrics are held fixed across models. Hyperparameters and checkpoints are selected on the validation split, and final results are reported on the held-out test split.

The primary metrics are average displacement error (ADE) and final displacement error (FDE), measured in meters:

$$\mathrm{ADE} = \frac{1}{NT}\sum_{i=1}^{N}\sum_{t=1}^{T}\left\|\hat{\mathbf{y}}_{i,t} - \mathbf{y}_{i,t}\right\|_2, \qquad \mathrm{FDE} = \frac{1}{N}\sum_{i=1}^{N}\left\|\hat{\mathbf{y}}_{i,T} - \mathbf{y}_{i,T}\right\|_2. \tag{2}$$

where N is the number of test samples and $T = T_f$ is the prediction length. Predictions and targets are denormalized to the target-vessel-centered metric frame before evaluation.

Beyond full-horizon ADE and FDE, we evaluate both tracks at multiple intermediate prediction horizons. Owing to space constraints, the main paper reports only representative checkpoints, including 3- and 6-minute ADE for Track A and selected long-horizon results for Track B. Complete per-horizon results for all evaluated models and regions are provided in the public benchmark release. We further stratify ADE by trajectory difficulty, scene type, and neighboring-vessel count. For methods that generate multiple future trajectories, the evaluation toolkit additionally supports

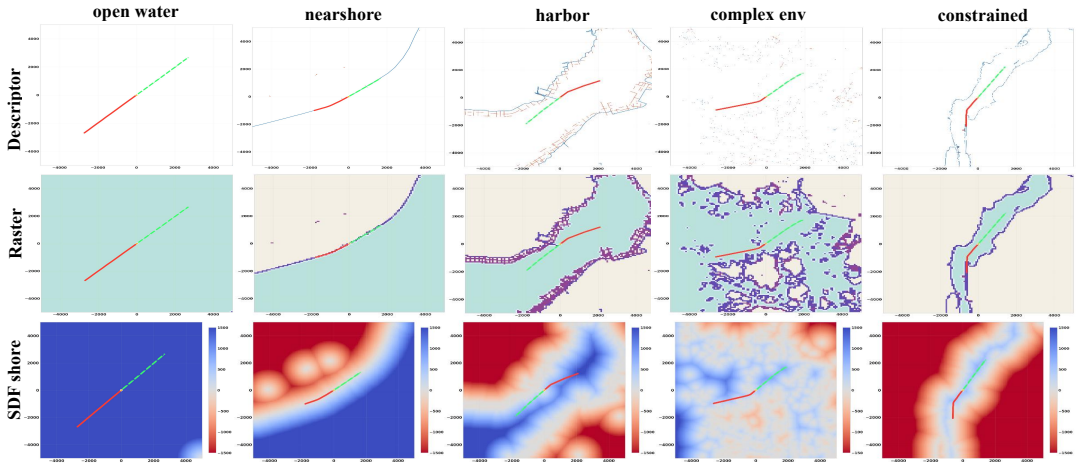


Figure 5: Representative environmental-context samples. Columns show different maritime scenes; rows show descriptor(vector geometry), water–land rasters, and shoreline signed-distance fields.

minADE@K and minFDE@K, computed as the minimum error over the K predicted futures for each sample.

4.2 Reference Models

The main comparison contains multiple reference systems selected to cover complementary motion assumptions, temporal architectures, and context representations.

Physics and classical machine learning. Constant Velocity extrapolates the mean velocity over the final three observed steps, whereas Dead Reckoning integrates the final reported speed over ground and course over ground. Random Forest [3] predicts each future position from flattened trajectory and motion features using a separate two-dimensional regressor for each prediction step.

Trajectory-only models. We include a two-layer LSTM encoder–decoder with 256 hidden units [16], a Temporal Convolutional Network with dilated causal convolutions [2], and a non-autoregressive Transformer that predicts the complete future sequence in one forward pass [12, 46]. These models represent recurrent, convolutional, and attention-based temporal architectures, respectively.

Neighboring-vessel context. Both neighboring-vessel models use the same LSTM trajectory encoder and a shared MLP to embed each valid neighbor. The pooling model aggregates these embeddings into a single context vector. The gated attention model instead performs validity-masked cross-attention at each decoder step, incorporates CPA, TCPA, and relative-speed attributes, and uses a neighbor-count gate to suppress the interaction pathway when no valid neighbors are present.

Environmental context. The descriptor model conditions the decoder at each prediction step through feature-wise linear modulation (FiLM) [35]. Raster-based models form a controlled 2×2 comparison of {binary raster, SDF} × {global pooling, spatial attention}. The binary raster provides discrete occupancy information, whereas the signed-distance fields(SDF) encode continuous distances to shoreline and navigable-region boundaries. Representative environmental representations across different maritime scenes are shown in Figure 5. Global-pooling models compress the CNN feature map into one vector; spatial-attention models retain the feature map and query it at each decoder step. This design separates the effect of environmental representation from that of context aggregation.

Joint context. The descriptor-based joint model combines neighboring-vessel attention with FiLM conditioning from the environmental descriptor. The SDF-based joint model combines gated neighboring-vessel attention with spatial attention over the SDF feature map. These models evaluate whether interaction and geographic information provide complementary forecasting cues.

4.3 Training and Statistical Protocol

Neural models are optimized with AdamW [22] using a learning rate of 5×10^{-4}, weight decay of 10^{-4}, a cosine learning-rate schedule, Huber loss with $\delta = 1$ in normalized coordinate space [17], and a batch size of 256. Training runs for at most 80 epochs and stops after 20 epochs without improvement in validation loss. For autoregressive recurrent decoders, teacher forcing is linearly annealed to zero over the first 40% of training. For each training configuration, normalization statistics are estimated exclusively from its training split and applied unchanged to the corresponding validation and test samples. Checkpoints are selected by validation loss. Unless a multimodal head is explicitly enabled, each learned model outputs one deterministic future trajectory.

5 In-Domain Results

We summarize representative in-domain results for DMA Track A, regional variation on Track A, and the long-horizon Track B. Models are trained and selected on the corresponding regional training and validation sets and evaluated on the vessel-disjoint test set using the recommended temporally consistent subset. Complete model–region and intermediate-horizon results are provided in the benchmark release.

5.1 Short-Horizon Track A

Dead Reckoning remains a strong reference at 91.6 m ADE, outperforming Random Forest and the plain LSTM. TCN is the strongest

Table 3: DMA Track A in-domain results. For learned models, ADE and FDE are reported as mean ± standard deviation across 5-seeds; temporal, difficulty, and scene entries report seed-averaged ADE. All values are in meters and lower is better. The best mean in each column is shown in bold.

				Temporal		Difficulty			Scene		
Category	**Model**	**ADE↓**	**FDE↓**	**3 min**	**6 min**	**Easy**	**Medium**	**Hard**	**Open**	**Nearshore**	**Harbor**
Physics	Constant Velocity	98.4	243.6	18.8	45.9	29.0	107.8	404.8	94.5	187.0	201.4
	Dead Reckoning	91.6	231.9	16.0	41.3	**26.5**	98.5	382.5	88.0	171.9	174.7
Classical ML	Random Forest	96.1	245.0	16.7	43.0	43.7	100.9	332.4	93.5	149.1	148.8
Trajectory only	LSTM	93.2 ±0.5	236.0 ±2.1	18.9	42.8	42.7	98.6	319.3	93.2	167.9	154.9
	TCN	87.0 ±0.7	222.0 ±1.4	**15.9**	**40.5**	36.8	**94.4**	307.7	87.0	145.2	140.7
	Transformer-NAR	95.7 ±1.6	234.7 ±3.5	23.1	46.4	46.8	101.7	313.4	95.7	149.7	158.8
Neighbor context	LSTM + Neighbor Pool	91.1 ±1.1	229.8 ±2.4	18.6	42.1	40.2	98.3	315.5	87.3	168.0	147.9
	LSTM + Gated Neighbor Attention	94.3 ±0.2	238.3 ±1.4	18.9	43.6	44.2	99.0	319.8	90.6	168.5	155.5
Environment context	LSTM + Descriptor FiLM	87.0 ±0.2	213.0 ±0.9	21.0	42.3	39.0	98.4	290.2	83.5	155.2	148.4
	LSTM + Binary Raster	86.2 ±0.4	211.2 ±1.0	18.7	40.9	38.8	97.8	279.5	**82.2**	**144.9**	140.7
	LSTM + Binary Spatial Attention	89.0 ±1.2	219.6 ±1.2	18.4	42.4	42.3	99.1	288.1	85.9	156.0	145.7
	LSTM + SDF	**85.5** ±0.9	**210.3** ±2.4	17.8	41.0	38.9	96.6	282.2	82.3	157.9	**134.6**
	LSTM + SDF Spatial Attention	87.2 ±0.2	215.0 ±1.2	18.7	42.0	41.5	97.5	281.9	84.3	149.6	149.4
Joint context	LSTM + Neighbor Attn + Descriptor	87.0 ±0.4	213.4 ±0.6	20.3	42.0	39.5	97.9	288.7	83.5	152.9	159.6
	LSTM + Gated Neighbor Attn + SDF	87.4 ±0.4	215.1 ±2.1	18.6	42.0	42.9	97.9	**275.8**	84.6	148.5	141.2

trajectory-only model, achieving 87.0 ± 0.7 m ADE, as shown in Table 3. Environment-aware models obtain the lowest aggregate errors: LSTM+SDF achieves 85.5 ± 0.9 m ADE and 210.3 ± 2.4 m FDE, followed closely by Binary Raster at 86.2 ± 0.4 m ADE. Spatial attention does not provide a consistent improvement. It increases ADE from 86.2 to 89.0 m for binary rasters and from 85.5 to 87.2 m for SDFs. The results therefore support the utility of environmental conditioning, but do not establish a uniform advantage for either spatial attention or SDF representation. The preferred representation also varies by scene. Binary Raster achieves the lowest nearshore ADE at 144.9 m, whereas SDF performs best in harbor scenes at 134.6 m. Because the harbor cohort contains only 15 samples, this comparison is diagnostic rather than conclusive. Even the best hard-tier result remains 275.8 m ADE, confirming the difficulty of strongly turning trajectories.

Neighboring-vessel context. Neighbor Pool modestly improves over the LSTM (91.1 versus 93.2 m ADE), whereas Gated Neighbor Attention does not (94.3 m). However, 79.5% of the DMA test samples contain no neighboring vessel within 3 km, so aggregate results are dominated by isolated trajectories. Neighbor-count-stratified results are provided in the public benchmark release.

Seed stability. Seed-level variation is generally modest, with ADE standard deviations between 0.2 and 1.6 m across learned models. The differences among SDF (85.5 ± 0.9 m), Binary Raster (86.2 ± 0.4 m), TCN (87.0 ± 0.7 m), and Descriptor FiLM (87.0 ± 0.2 m) are therefore small relative to their variability. Close rankings should consequently be interpreted as comparable performance rather than robust superiority.

Regional Variation on Track A. Model rankings vary substantially across operating regimes. On NOAA, TCN performs best at 92.8 m ADE, while SDF reaches 100.4 m, indicating limited aggregate benefit from environmental context in the predominantly open-water setting. On Norway, Dead Reckoning achieves 108.4 m ADE and outperforms the best learned model (SDF, 127.5 m). In contrast, SDF achieves 151.8 m on Piraeus, improving over TCN at 169.1 m by 17.3 m. Environmental context therefore provides its clearest benefit where geographic constraints are informative, rather than uniformly across regions.

Table 4: Track B full-horizon in-domain results (30 min → 60 min) on DMA (N=6,000) and NOAA (N=4,148). For ADE and FDE (m), lower is better. Best values are shown in bold.

	DMA Track B		NOAA Track B	
Model	**ADE↓**	**FDE↓**	**ADE↓**	**FDE↓**
LSTM	658.5 ±2.2	1539.2 ±9.5	1361.1 ±5.3	3055.3 ±15.1
GRU	642.6 ±3.8	**1486.8** ±7.6	1208.1 ±6.2	2693.8 ±13.5
BiLSTM	651.5 ±2.1	1536.7 ±7.3	1358.9 ±4.8	3022.6 ±16.3
TCN	**635.1** ±2.3	1489.6 ±5.8	**1136.5** ±4.4	**2575.2** ±10.2
Transformer-NAR	680.4 ±1.9	1545.8 ±16.7	1247.9 ±3.8	2750.3 ±28.4
LSTM + Neighbor Pool	652.0 ±3.4	1543.8 ±12.4	1395.1 ±6.9	3146.8 ±32.1
LSTM + Binary Raster	643.1 ±2.9	1510.6 ±10.1	1872.7 ±7.9	4189.1 ±30.5
LSTM + Binary SpAttn	659.3 ±4.8	1544.4 ±6.2	1232.8 ±7.4	2730.7 ±23.1
LSTM + SDF	643.7 ±2.2	1521.5 ±10.6	1369.4 ±5.8	3085.9 ±22.7
LSTM + G-Nbr Attn + SDF	663.1 ±4.4	1551.1 ±15.1	1299.5 ±8.3	2887.7 ±32.6

5.2 Long-Horizon Track B

Track B extends prediction to 60 minutes. Table 4 reports full-horizon results for DMA and NOAA, the two largest Track B test cohorts; complete four-region and intermediate-horizon results are provided in the benchmark release.

TCN obtains the lowest ADE on both DMA and NOAA, reaching 635.1 and 1,136.5 m, respectively. GRU achieves the lowest DMA FDE at 1,486.8 m, narrowly outperforming TCN at 1,489.6 m, whereas TCN remains best on NOAA for both metrics. Environmental models remain close to TCN on DMA but degrade more substantially on NOAA, confirming that model rankings depend on both horizon and regional operating conditions.

On DMA, SDF reduces ADE relative to the same-backbone LSTM from 658.5 to 643.7 m, corresponding to a 2.2% improvement at 60 minutes, compared with approximately 10% over the first 10 minutes. This attenuation is consistent with the fixed, anchor-centered context: its contribution decreases as vessels move beyond the spatial support available at the observation endpoint.

6 Cross-Region Transfer

All regions share the same construction pipeline, forecasting protocols, and target-centered coordinate frame. Normalization statistics are estimated from each training pool and applied unchanged at test time, isolating geographic and operational distribution shift. We examine Track A zero-shot transfer and multi-source source-removal ablations; complete results for both tracks are provided in the benchmark release.

6.1 DMA-to-NOAA Zero-Shot Transfer

Without NOAA fine-tuning, ADE increases from 87.0 to 101.5 m for TCN, from 87.0 to 107.4 m for Descriptor FiLM, and from 85.5 to 105.5 m for SDF. Dead Reckoning similarly increases from 91.6 to 106.5 m, confirming a clear regional shift under otherwise identical evaluation protocols. TCN achieves the lowest aggregate NOAA ADE. On nearshore samples, however, SDF performs best at 203.0 m, compared with 222.1 m for TCN and 251.5 m for Dead Reckoning. Environmental context therefore remains useful under geographic shift when coastline geometry constrains vessel motion.

6.2 Multi-Source Training and Source Removal

Table 5 and Figure 6 compare training on all four regions with source-removal variants. Each removed source is excluded from both training and evaluation; the remaining cells measure its contribution to the retained regions.

Combined training is competitive but not uniformly beneficial. TCN achieves 88.9 and 92.9 m ADE on DMA and NOAA, close to its in-domain results of 87.0 and 92.8 m. On Piraeus, combined training improves TCN from 169.1 to 162.7 m and SDF from 151.8 to 145.9 m. Combined SDF also improves NOAA from 100.4 to 98.4 m, but degrades DMA from 85.5 to 89.3 m.

Source contributions are strongly asymmetric. Removing DMA degrades all three models on most retained regions, whereas removing Norway improves both context-aware models on every retained target. Removing Piraeus also reduces Norway ADE from 125.0 to 112.9 m for TCN and from 127.5 to 123.4 m for SDF. Thus, additional regional data can introduce negative transfer, and effective source selection depends on both the target regime and model architecture. The same qualitative behavior is also observed on Track B.

Table 5: Track A ADE (m) under multi-source and source-removal training. Values are mean ± standard deviation over five seeds; dashes denote excluded sources.

Training pool	Model	DMA	NOAA	Piraeus	Norway
Combined (all 4)	TCN	88.9 ±0.7	92.9 ±0.8	162.7 ±0.8	125.0 ±0.9
	LSTM + SDF	89.3 ±1.4	98.4 ±0.9	145.9 ±1.6	127.5 ±1.4
	LSTM + G-Nbr Attn + SDF	92.5 ±0.7	99.3 ±1.0	152.4 ±1.3	127.7 ±0.8
LOSO (no DMA)	TCN	—	96.4 ±1.6	164.3 ±0.5	127.9 ±2.3
	LSTM + SDF	—	105.9 ±1.9	150.6 ±1.2	131.3 ±2.5
	LSTM + G-Nbr Attn + SDF	—	103.3 ±1.4	153.8 ±0.7	133.2 ±0.4
LOSO (no NOAA)	TCN	91.8 ±1.7	—	164.5 ±1.5	127.7 ±2.6
	LSTM + SDF	89.2 ±1.5	—	145.6 ±1.6	127.4 ±2.5
	LSTM + G-Nbr Attn + SDF	91.3 ±0.6	—	151.5 ±1.1	127.9 ±1.0
LOSO (no Piraeus)	TCN	87.9 ±0.4	91.7 ±0.4	—	112.9 ±0.7
	LSTM + SDF	92.9 ±1.3	101.3 ±1.4	—	123.4 ±2.9
	LSTM + G-Nbr Attn + SDF	91.9 ±1.8	100.5 ±1.5	—	123.8 ±2.5
LOSO (no Norway)	TCN	88.6 ±1.0	92.2 ±0.7	163.9 ±0.8	—
	LSTM + SDF	86.6 ±1.0	95.6 ±0.2	142.1 ±0.8	—
	LSTM + G-Nbr Attn + SDF	90.4 ±0.8	97.6 ±0.9	149.4 ±2.4	—

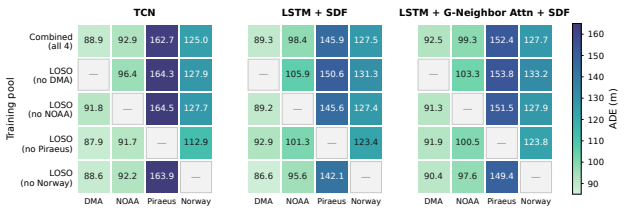


Figure 6: Track A ADE under multi-source and source-removal training. Blank cells denote excluded sources.

7 Conclusion

We presented EnvShip, a unified framework for context-aware and cross-region vessel trajectory forecasting. EnvShip processes four public AIS sources through a shared pipeline and provides two multi-horizon tracks with vessel-disjoint splits, sample-aligned environmental, interaction, and meteorological context, and transparent quality-control metadata.

Evaluation across regions, horizons, scene types, and training-source compositions shows that forecasting performance depends strongly on the operating regime. Physics-based and trajectory-only models remain competitive in regular and open-water settings, whereas environmental context is most useful when geographic constraints are informative, its preferred representation nevertheless varies across scenes. Neighboring-vessel context provides clearer benefits in interaction-rich subsets than in aggregate evaluation. Multi-source training can improve geographically distinct targets, but mismatched sources may introduce negative transfer. These findings motivate scene-, interaction-, and source-stratified reporting rather than relying on a single aggregate ranking. Remaining limitations include regional and seasonal imbalance, sparse interaction-rich cases, and the inherent incompleteness of public AIS data. The benchmark pipeline, evaluation tools, and processed data are available through https://github.com/mark000071/Envship_Framework_vessel_traj_pred and https://huggingface.co/datasets/mark000071/envship_v2_datasets.

References

[1] Alexandre Alahi, Kratarth Goel, Vignesh Ramanathan, Alexandre Robicquet, Li Fei-Fei, and Silvio Savarese. 2016. Social LSTM: Human Trajectory Prediction in Crowded Spaces. In *Proceedings of the IEEE Conference on Computer Vision and Pattern Recognition (CVPR)*. 961–971.

[2] Shaojie Bai, J. Zico Kolter, and Vladlen Koltun. 2018. An Empirical Evaluation of Generic Convolutional and Recurrent Networks for Sequence Modeling. *arXiv preprint arXiv:1803.01271* (2018).

[3] Leo Breiman. 2001. Random Forests. *Machine Learning* 45, 1 (2001), 5–32.

[4] Holger Caesar, Varun Bankiti, Alex H. Lang, Sourabh Vora, Venice Erin Liong, Qiang Xu, Anush Krishnan, Yu Pan, Giancarlo Baldan, and Oscar Beijbom. 2020. nuScenes: A Multimodal Dataset for Autonomous Driving. In *Proceedings of the IEEE/CVF Conference on Computer Vision and Pattern Recognition (CVPR)*. 11621–11631.

[5] Samuele Capobianco, Leonardo M. Millefiori, Nicola Forti, Paolo Braca, and Peter Willett. 2021. Deep Learning Methods for Vessel Trajectory Prediction Based on Recurrent Neural Networks. *IEEE Trans. Aerospace Electron. Systems* 57 (2021), 4329–4346. doi:10.1109/TAES.2021.3096873

[6] Ming-Fang Chang, John Lambert, Patsorn Sangkloy, Jagjeet Singh, Slawomir Bak, Andrew Hartnett, De Wang, Peter Carr, Simon Lucey, Deva Ramanan, and James Hays. 2019. Argoverse: 3D Tracking and Forecasting with Rich Maps. In *Proceedings of the IEEE/CVF Conference on Computer Vision and Pattern Recognition (CVPR)*. 8748–8757. doi:10.1109/CVPR.2019.00895

[7] Changhe Chen, Mozhgan Pourkeshavarz, and Amir Rasouli. 2024. CRITERIA: A New Benchmarking Paradigm for Evaluating Trajectory Prediction Models for Autonomous Driving. In *2024 IEEE International Conference on Robotics and Automation (ICRA)*. IEEE, 8265–8271. doi:10.1109/ICRA57147.2024.10610911

[8] X. Chen, J. Ling, Y. Yang, H. Zheng, P. Xiong, O. Postolache, and Y. Xiong. 2020. Ship Trajectory Reconstruction from AIS Sensory Data via Data Quality Control and Prediction. *Mathematical Problems in Engineering* 2020 (2020), 7191296. doi:10.1155/2020/7191296

[9] Danish Maritime Authority. 2026. AIS Data. https://www.dma.dk/safety-at-sea/navigational-information/ais-data Accessed: 2026-03-31.

[10] figshare. 2019. Ushant AIS Dataset. https://figshare.com/articles/dataset/Ushant_AIS_dataset/8966273 Accessed: 2026-03-31.

[11] Miao Gao, Maohan Liang, Anmin Zhang, Yingjun Hu, and Jixiang Zhu. 2024. Multi-ship encounter situation graph structure learning for ship collision avoidance based on AIS big data with spatio-temporal edge and node attention graph convolutional networks. *Ocean Engineering* 301 (2024), 117605.

[12] Francesco Giuliari, Irtiza Hasan, Marco Cristani, and Fabio Galasso. 2021. Transformer Networks for Trajectory Forecasting. In *Proceedings of the International Conference on Pattern Recognition*. 10335–10342.

[13] Agrim Gupta, Justin Johnson, Li Fei-Fei, Silvio Savarese, and Alexandre Alahi. 2018. Social GAN: Socially Acceptable Trajectories With Generative Adversarial Networks. In *Proceedings of the IEEE/CVF Conference on Computer Vision and Pattern Recognition (CVPR)*. 2255–2264.

[14] Mordechai Haklay and Patrick Weber. 2008. OpenStreetMap: User-Generated Street Maps. *IEEE Pervasive Computing* 7, 4 (2008), 12–18.

[15] Sandro Hauri, Nemanja Djuric, Vladan Radosavljevic, and Slobodan Vucetic. 2021. Multi-Modal Trajectory Prediction of NBA Players. In *Proceedings of the IEEE/CVF Winter Conference on Applications of Computer Vision*. 1640–1649. doi:10.1109/WACV48630.2021.00168

[16] Sepp Hochreiter and Jürgen Schmidhuber. 1997. Long Short-Term Memory. *Neural Computation* 9, 8 (1997), 1735–1780.

[17] Peter J. Huber. 1964. Robust Estimation of a Location Parameter. *The Annals of Mathematical Statistics* 35, 1 (1964), 73–101.

[18] Alon Lerner, Yiorgos Chrysanthou, and Dani Lischinski. 2007. Crowds by Example. *Computer Graphics Forum* 26, 3 (2007), 655–664. doi:10.1111/j.1467-8659.2007.01089.x

[19] Huanhuan Li, Hang Jiao, and Zaili Yang. 2023. Ship trajectory prediction based on machine learning and deep learning: A systematic review and methods analysis. *Engineering Applications of Artificial Intelligence* 126 (2023), 107062.

[20] Maohan Liang, Ryan Wen Liu, Yang Zhan, Huanhuan Li, Fenghua Zhu, and Fei-Yue Wang. 2022. Fine-grained vessel traffic flow prediction with a spatio-temporal multigraph convolutional network. *IEEE Transactions on Intelligent Transportation Systems* 23, 12 (2022), 23694–23707.

[21] R. W. Liu, M. Liang, J. Nie, W. Y. B. Lim, Y. Zhang, and M. Guizani. 2022. Deep Learning-Powered Vessel Trajectory Prediction for Improving Smart Traffic Services in Maritime Internet of Things. *IEEE Transactions on Network Science and Engineering* 9 (2022), 3080–3094. doi:10.1109/TNSE.2022.3140529

[22] Ilya Loshchilov and Frank Hutter. 2019. Decoupled Weight Decay Regularization. In *International Conference on Learning Representations*.

[23] Kun Ma, Qilong Han, and Jingzheng Yao. 2025. Multi-Ship Future Interaction Trajectory Prediction via Pre-Initializer Diffusion Model. In *Proceedings of the 24th International Conference on Autonomous Agents and Multiagent Systems*. 1408–1417.

[24] Kun Ma, Qilong Han, Jingzheng Yao, Changmao Wu, and Yuntao Zhang. 2025. DDA: Distillation-Driven Acceleration of the Reverse Diffusion Process for Stochastic Multi-Ship Trajectory Prediction. In *ICASSP 2025 - 2025 IEEE International Conference on Acoustics, Speech and Signal Processing (ICASSP)*. 1–5. doi:10.1109/ICASSP49660.2025.10889007

[25] MarineCadastre.gov. 2026. AccessAIS. https://marinecadastre.gov/accessais/. Accessed: 2026-03-30.

[26] Saeed Mehri, Ali A. Alesheikh, and Amin Basiri. 2021. A Contextual Hybrid Model for Vessel Movement Prediction. *IEEE Access* 9 (2021), 45600–45613. doi:10.1109/ACCESS.2021.3066463

[27] Abduallah Mohamed, Kun Qian, Mohamed Elhoseiny, and Christian Claudel. 2020. Social-stgcnn: A social spatio-temporal graph convolutional neural network for human trajectory prediction. In *Proceedings of the IEEE/CVF conference on computer vision and pattern recognition*. 14424–14432.

[28] Brendan Murray and Lokukaluge P. Perera. 2021. An AIS-Based Deep Learning Framework for Regional Ship Behavior Prediction. *Reliability Engineering & System Safety* 215 (2021), 107819. doi:10.1016/j.ress.2021.107819

[29] Jiquan Ngiam, Vijay Vasudevan, Benjamin Caine, Zheng Zhang, H.-T. L. Chiang, et al. 2022. Scene Transformer: A Unified Architecture for Predicting Future Trajectories of Multiple Agents. In *ICLR*.

[30] Duong Nguyen and Ronan Fablet. 2024. TrAISformer: A Transformer Network for AIS-Based Vessel Trajectory Prediction. *IEEE Access* (2024), 21596–21609. doi:10.1109/ACCESS.2024.3349957

[31] NOAA Office for Coastal Management and Bureau of Ocean Energy Management. 2023. Frequently Asked Questions: AIS Data and Tools. https://coast.noaa.gov/data/marinecadastre/ais/faq.pdf. Accessed: 2026-03-30.

[32] Norwegian Coastal Administration. 2025. AIS Open Data via Kystdatahuset. Kystdatahuset. https://kystdatahuset.no/ August–September 2025 extracts; accessed October 2025.

[33] OpenStreetMap contributors. 2026. OpenStreetMap Planet Dump. OpenStreetMap Foundation, https://planet.openstreetmap.org/. Open Database License.

[34] Stefano Pellegrini, Andreas Ess, Konrad Schindler, and Luc Van Gool. 2009. You'll Never Walk Alone: Modeling Social Behavior for Multi-Target Tracking. In *Proceedings of the IEEE International Conference on Computer Vision*. 261–268. doi:10.1109/ICCV.2009.5459260

[35] Ethan Perez, Florian Strub, Harm de Vries, Vincent Dumoulin, and Aaron Courville. 2018. FiLM: Visual Reasoning with a General Conditioning Layer. In *Proceedings of the AAAI Conference on Artificial Intelligence*.

[36] Huimin Qiang, Zhiyuan Guo, Shiyuan Xie, and Xiaodong Peng. 2023. MSTFormer: Motion Inspired Spatial-temporal Transformer with Dynamic-aware Attention for Long-term Vessel Trajectory Prediction. *arXiv preprint arXiv:2303.11540* (2023).

[37] Cyril Ray, Richard Dréo, Elena Camossi, Anne-Laure Jousselme, and Clément Iphar. 2019. Heterogeneous Integrated Dataset for Maritime Intelligence, Surveillance, and Reconnaissance. *Data in Brief* 25 (2019), 104141. doi:10.1016/j.dib.2019.104141

[38] Alexandre Robicquet, Amir Sadeghian, Alexandre Alahi, and Silvio Savarese. 2016. Learning Social Etiquette: Human Trajectory Understanding in Crowded Scenes. In *Computer Vision – ECCV 2016*. Springer, 549–565. doi:10.1007/978-3-319-46484-8_33

[39] H Rong, AP Teixeira, and C Guedes Soares. 2019. Ship trajectory uncertainty prediction based on a Gaussian Process model. *Ocean Engineering* 182 (2019), 499–511.

[40] Tim Salzmann, Boris Ivanovic, Punarjay Chakravarty, and Marco Pavone. 2020. Trajectron++: Dynamically-Feasible Trajectory Forecasting with Heterogeneous Data. In *Proceedings of the European Conference on Computer Vision (ECCV)*. doi:10.1007/978-3-030-58523-5_40

[41] Huang Tang, Yong Yin, and Helong Shen. 2022. A model for vessel trajectory prediction based on long short-term memory neural network. *Journal of Marine Engineering & Technology* 21, 3 (2022), 136–145.

[42] Technical University of Denmark. 2023. AIS Trajectories from Danish Waters for Abnormal Behavior Detection. https://data.dtu.dk/collections/AIS_Trajectories_from_Danish_Waters_for_Abnormal_Behavior_Detection/6287841 Accessed: 2026-03-31.

[43] Andreas Tritsarolis, Yannis Kontoulis, and Yannis Theodoridis. 2022. The Piraeus AIS Dataset for Large-Scale Maritime Data Analytics. *Data in Brief* 40 (2022), 107782. doi:10.1016/j.dib.2021.107782 Associated data record: Zenodo, doi:10.5281/zenodo.6323416.

[44] Enmei Tu, Guanghao Zhang, Lily Rachmawati, Eshan Rajabally, and Guang-Bin Huang. 2018. Exploiting AIS Data for Intelligent Maritime Navigation: A Comprehensive Survey From Data to Methodology. *IEEE Transactions on Intelligent Transportation Systems* 19, 5 (2018), 1559–1582. doi:10.1109/TITS.2017.2724551

[45] United Nations Conference on Trade and Development. 2025. *Review of Maritime Transport 2025: Staying the Course in Turbulent Waters*. Technical Report UNCTAD/RMT/2025. United Nations, Geneva. https://unctad.org/publication/review-maritime-transport-2025

[46] Ashish Vaswani, Noam Shazeer, Niki Parmar, Jakob Uszkoreit, Llion Jones, Aidan N. Gomez, Łukasz Kaiser, and Illia Polosukhin. 2017. Attention Is All You Need. In *Advances in Neural Information Processing Systems*. 5998–6008.

[47] Benjamin Wilson, William Qi, Tanmay Agarwal, John Lambert, Jagjeet Singh, Siddhesh Khandelwal, Bowen Pan, Ratnesh Kumar, Andrew Hartnett, Jhony Kaesemodel Pontes, Deva Ramanan, Peter Carr, and James Hays. 2021. Argoverse 2: Next Generation Datasets for Self-Driving Perception and Forecasting. In *Proceedings of the Neural Information Processing Systems Track on Datasets and Benchmarks*.

[48] Lan You, Siyu Xiao, Qingxi Peng, Christophe Claramunt, Xuewei Han, Zhengyi Guan, and Jiahe Zhang. 2020. St-seq2seq: A spatio-temporal feature-optimized seq2seq model for short-term vessel trajectory prediction. *IEEE Access* 8 (2020), 218565–218574.

[49] Ye Yuan, Xinshuo Weng, Yanglan Ou, and Kris Kitani. 2021. AgentFormer: Agent-Aware Transformers for Socio-Temporal Multi-Agent Forecasting. In *Proceedings of the IEEE/CVF International Conference on Computer Vision (ICCV)*. 9793–9803.

[50] Zenodo. 2018. Final Dataset of Trajectory Synopses over AIS Kinematic Messages in Brest Area. doi:10.5281/zenodo.2563256

[51] J. Zhang, X. Ren, H. Li, and Z. Yang. 2022. Incorporation of Deep Kernel Convolution into Density Clustering for Shipping AIS Data Denoising and Reconstruction. *Journal of Marine Science and Engineering* 10, 9 (2022), 1319. doi:10.3390/jmse10091319

[52] Liye Zhang, Qiang Meng, Zhe Xiao, and Xiuju Fu. 2018. A Novel Ship Trajectory Reconstruction Approach Using AIS Data. *Ocean Engineering* 159 (2018), 165–174. doi:10.1016/j.oceaneng.2018.03.085

[53] X. Zhang, X. Fu, Z. Xiao, H. Xu, and Z. Qin. 2022. Vessel Trajectory Prediction in Maritime Transportation: Current Approaches and Beyond. *IEEE Transactions on Intelligent Transportation Systems* 23 (2022), 19980–19998. doi:10.1109/TITS.2022.3192574

[54] Zikang Zhou, Li Ye, Jiajun Wang, Kun Wu, and Kejie Lu. 2022. HiVT: Hierarchical Vector Transformer for Multi-Agent Motion Prediction. In *CVPR*.

Table 6: Parameters used for standard-track curation and auditing.

Component	Setting
Split assignment	Deterministic MMSI hash; 80/10/10 train/validation/test split
Difficulty allocation	35/40/25 easy/medium/hard
Training caps	At most 55 windows per vessel and 12 per continuous segment
Validation/test caps	At most 70 windows per vessel and 20 per continuous segment
Within-segment spacing	Anchor-time separation of at least $\Delta_{\min}$, defined in the released configuration
Recommended OSM criterion	Maximum inland depth no greater than 30 m and fewer than three consecutive inland points

A Dataset Construction and Curation Details

This appendix specifies how the quality-screened regional cores are converted into the released standard tracks. Source adapters, record-level filtering, trajectory segmentation, interpolation, and resampling follow the shared pipeline described in the main paper and are not repeated here.

A.1 Regional Cores and Track Eligibility

A regional core is the set of quality-screened candidate windows obtained before standard-track curation. Each candidate retains its MMSI, continuous-segment identifier, anchor time, vessel class, train/validation/test assignment, trajectory-difficulty tier, and sample-level quality metadata. The regional cores support alternative task construction, whereas the standard tracks provide fixed subsets for controlled model comparison.

A Track A candidate must contain 30 observed and 30 future positions, corresponding to 10 minutes of observation and 10 minutes of prediction. A Track B candidate must contain 90 observed and 180 future positions, corresponding to 30 minutes of observation and 60 minutes of prediction. Candidates with an incomplete observation–prediction interval or a failed trajectory-level quality check are excluded before quota allocation.

Table 6 summarizes the parameters specific to standard-track curation and the recommended OpenStreetMap audit.

A.2 Core-to-Track Curation

Curation is performed independently within each source and split. The vessel-disjoint assignment established before curation is preserved throughout the procedure; samples are never reassigned across train, validation, and test sets. Table 7 summarizes the selection process.

Vessel-class allocation uses the shared taxonomy defined in the main paper. Class proportions are controlled at the benchmark level rather than imposed independently on every region. This preserves regional differences in fleet composition and avoids exhausting vessel classes that are uncommon in a particular source.

Difficulty tiers are defined by the turning-based score in Eq. 1. Candidates are classified as easy ($D_i < 5$), medium ($5 \le D_i < 12$), or hard ($D_i \ge 12$), with a target allocation of 35/40/25. Because the score depends on the complete observed-and-future trajectory, it is used only for dataset curation and stratified evaluation and is never provided to a forecasting model.

The vessel and segment caps reduce repeated sampling of similar motion from the same vessel or continuous segment. For any two selected windows i and j from the same segment,

$$|a_i - a_j| \ge \Delta_{\min},$$

where a_i and a_j are their anchor times. The value of $\Delta_{\min}$ for each curation configuration is stored in the version-controlled release files.

Track A reaches the fixed source allocation of 150,000 samples from DMA and 60,000 samples from each of NOAA, Piraeus, and Norway. Track B contains 106,857 samples. Its regional imbalance reflects the availability of continuous 270-position windows rather than post-hoc filtering based on model performance. Exact source–split counts are reported in Table 2.

A.3 OpenStreetMap Temporal-Consistency Audit

OpenStreetMap geometry may postdate the corresponding AIS observations. Coastal infrastructure added after the observation period, such as reclaimed land, piers, and breakwaters, can therefore cause historically valid vessel trajectories to appear inland relative to a later map snapshot.

Let $d_{i,t}^{\text{in}} \ge 0$ denote the inland depth of trajectory point t in sample i, as derived from the shoreline signed-distance field, with zero assigned to points that are not inland. The audit records

$$d_i^{\max} = \max_t d_{i,t}^{\text{in}}, \qquad n_i^{\text{in}} = \sum_t \mathbf{1}\left[d_{i,t}^{\text{in}} > 0\right], \qquad \ell_i^{\text{in}} = \text{LongestRun}_t\, \mathbf{1}\left[d_{i,t}^{\text{in}} > 0\right].$$

Here, $d_i^{\max}$ is the maximum inland penetration, n_i^{in} is the total number of inland points, and ℓ_i^{in} is the longest consecutive run of inland points. A sample belongs to the recommended temporally consistent subset when

$$d_i^{\max} \le 30\,\text{m} \qquad \text{and} \qquad \ell_i^{\text{in}} < 3.$$

The audit does not remove samples from the release. The complete set, the pass/fail flag, and all diagnostic values are provided so that users can apply alternative criteria. The recommended criterion retains 326,316 of the 330,000 Track A samples and 99,191 of the 106,857 Track B samples.

For Piraeus, whose AIS observations were collected in 2019, environmental context and the corresponding audit use a pinned OpenStreetMap snapshot dated 2020-01-01.

The target trajectory and split assignment are fixed before context records are attached. Environmental context, neighboring-vessel features, and meteorological attributes use only information available at or before the anchor time. The temporal-consistency audit examines the complete trajectory only to generate quality diagnostics and the recommended-subset flag; these values are not used as forecasting inputs. Consequently, neither context construction nor auditing changes split membership or introduces prediction-interval information into the model inputs.

B Reference Models and Context Packages

This appendix provides implementation details for the reference models and defines the released environmental, neighboring-vessel,

Table 7: Procedure for converting regional-core candidates into the released standard tracks.

Step	Stage	Rule	Output
1	Protocol eligibility	Retain candidates containing the complete Track A or Track B observation–prediction interval and satisfying all trajectory-level quality checks.	Track-specific candidate pools
2	Split preservation	Preserve the deterministic MMSI-based split assignment so that no vessel occurs in more than one split.	Vessel-disjoint source–split pools
3	Stratum construction	Group candidates by source, split, vessel class, and difficulty tier, and determine quotas subject to candidate availability.	Per-stratum candidate pools and quotas
4	Quality ordering	Order candidates within each stratum using interpolation ratio, displacement, path efficiency, speed variation, and temporal continuity.	Ranked candidates
5	Redundancy control	Enforce per-vessel and per-segment caps and require $\lvert a_i - a_j \rvert \geq \Delta_{\min}$ for selected windows from the same continuous segment.	Redundancy-controlled candidates
6	Quota completion	Select ranked candidates until the corresponding source–split quota is filled or the eligible pool is exhausted.	Standard-track samples
7	Context and audit	Link context records through the stable sample identifier and compute the OpenStreetMap temporal-consistency diagnostics.	Complete set and recommended subset

and meteorological context records. The common forecasting protocol, training procedure, and evaluation metrics are described in the main paper and are not repeated here.

B.1 Kinematic and Classical Baselines

Let $\mathbf{y}_{T_h}$ denote the final observed position, $\Delta t = 20\,\mathrm{s}$ the sampling interval, and $t = 1, \ldots, T_f$ a future step.

Constant Velocity. The velocity is estimated from the final $M = 3$ observed displacements:

$$\bar{\mathbf{v}} = \frac{1}{M} \sum_{k=T_h-M}^{T_h-1} \frac{\mathbf{y}_{k+1} - \mathbf{y}_k}{\Delta t}, \qquad \hat{\mathbf{y}}_{T_h+t} = \mathbf{y}_{T_h} + t\Delta t\, \bar{\mathbf{v}}.$$

Dead Reckoning. The final reported speed over ground is converted to meters per second and combined with the final course over ground expressed in the target-centered local frame:

$$\mathbf{v}^{\mathrm{DR}} = s_{T_h}\, \mathbf{u}(\psi_{T_h}), \qquad \hat{\mathbf{y}}_{T_h+t} = \mathbf{y}_{T_h} + t\Delta t\, \mathbf{v}^{\mathrm{DR}},$$

where s_{T_h} and ψ_{T_h} are the final observed SOG and COG, and $\mathbf{u}(\psi)$ is the corresponding unit direction vector.

Additional released baselines. The released baseline grid also includes Constant Acceleration, Random Forest, and XGBoost. Constant Acceleration fits independent quadratic functions to the final five observed x- and y-coordinates by least squares:

$$\mathbf{y}(\tau) = \mathbf{a} + \mathbf{b}\tau + \frac{1}{2}\mathbf{c}\tau^2,$$

and evaluates the fitted functions at future timestamps. Random Forest and XGBoost receive flattened trajectory and motion features. A separate two-dimensional regressor predicts each future step, so their outputs are non-autoregressive.

B.2 Neural and Context-Aware Implementations

Trajectory-only models. The LSTM, GRU, and bidirectional LSTM encoders use two recurrent layers with 256 hidden units. Their autoregressive decoders predict future displacements, which are accumulated from the final observed position. The TCN contains eight dilated causal-convolution layers with 128 channels and kernel size 3, followed by a full-horizon prediction head. Transformer-NAR encodes the complete observation sequence and predicts the full future sequence in one forward pass.

Neighbor-aware models. A shared multilayer perceptron embeds each valid neighboring vessel. Neighbor Pool aggregates the valid embeddings into a single permutation-invariant context vector. Gated Neighbor Attention instead applies validity-masked cross-attention at each decoder step using the neighbor embeddings together with CPA, TCPA, and relative-speed attributes. A neighbor-count gate suppresses this pathway when no valid neighbor is available.

Environmental models. The binary-raster and SDF models use the same three-stage CNN with feature widths 16, 32, and 64, producing a $64 \times 16 \times 16$ feature map. Global-pooling variants compress this map into one context vector. Spatial-attention variants retain the 16×16 spatial grid as 256 tokens and query these tokens at each decoder step.

The descriptor model applies feature-wise linear modulation to the decoder state:

$$\mathrm{FiLM}(\mathbf{h}_t, \mathbf{d}) = \boldsymbol{\gamma}(\mathbf{d}) \odot \mathbf{h}_t + \boldsymbol{\beta}(\mathbf{d}),$$

where $\mathbf{d}$ is the environmental descriptor and $\mathbf{h}_t$ is the decoder state.

Joint-context models. The descriptor-based joint model combines neighboring-vessel attention with descriptor FiLM. The SDF-based joint model combines gated neighboring-vessel attention with spatial attention over the SDF feature map. Matched variants use the same trajectory backbone, prediction target, normalization procedure, and training protocol, so their differences are limited to the supplied context pathway.

B.3 Environmental Context Package

Environmental context is constructed once at the anchor for both tracks. Each sample uses an axis-aligned $10\,\mathrm{km} \times 10\,\mathrm{km}$ crop in the target-centered local frame, represented on a 128×128 grid. The spatial resolution is therefore 78.125 m per pixel.

For a boundary set $\partial\Omega$, the signed-distance value at location $\mathbf{p}$ is

$$d(\mathbf{p}) = s(\mathbf{p}) \min_{\mathbf{q} \in \partial\Omega} \lVert \mathbf{p} - \mathbf{q} \rVert_2,$$

where $s(\mathbf{p}) \in \{-1, +1\}$ denotes the side of the boundary under the released sign convention. The shoreline and navigability SDFs use shoreline and navigable-region boundaries, respectively.

Table 8: Environmental context representations

Representation	Shape	Definition
Land mask	128×128	Pixels classified as land
Water mask	128×128	Pixels classified as water
Navigable-water mask	128×128	Water pixels associated with mapped navigable geometry
Natural-boundary mask	128×128	Coastlines and other natural boundaries
Man-made-boundary mask	128×128	Quays, piers, waterfronts, and related structures
Barrier mask	128×128	Breakwaters and other mapped barriers
Shoreline SDF	128×128	Signed distance to the nearest shoreline
Navigability SDF	128×128	Signed distance to the nearest navigable-region boundary
Scene descriptor	14	Scene encoding and scalar geometric and quality attributes
Vector geometry	Variable	Clipped shoreline and maritime-feature polylines

Table 9: Semantic organization of the environmental descriptor

Group	Dim.	Content
Scene encoding	5	Indicators for open-water, nearshore, harbor, complex-environment, and constrained scenes
Area ratios	2	Water and navigable-water proportions within the crop
Nearest distances	3	Distances to shoreline, navigable-region boundary, and barrier geometry
Boundary densities	3	Natural-, man-made-, and barrier-boundary densities
Context quality	1	Completeness or reliability of the constructed context
Total	14	Fixed ordering defined in the released schema

Table 10: Neighboring-vessel representations with $K_{\max} = 10$

Input	Shape	Content
Relative history	$K_{\max} \times T_h \times 2$	Neighbor positions relative to the target history
Relative velocity	$K_{\max} \times 2$	Δv_x and Δv_y at the anchor
Basic features	$K_{\max} \times 5$	Δx, Δy, Δv_x, Δv_y, and distance d
Extended features	$K_{\max} \times 8$	Basic features, CPA, TCPA, and relative-speed magnitude $\|\Delta \mathbf{v}\|_2$
Validity mask	$K_{\max}$	One for a valid neighbor and zero for padding

The 14-dimensional environmental descriptor follows the fixed ordering in Table 9.

Binary scene indicators are used directly. Continuous descriptor channels are standardized using statistics estimated only from the corresponding training pool:

$$\widetilde{z} = \frac{z - \mu_{\text{train}}}{\sigma_{\text{train}} + \varepsilon}.$$

The same statistics are applied unchanged to validation and test samples.

B.4 Neighboring-Vessel Context

At the anchor time, valid surrounding vessels are ordered by Euclidean distance to the target. The nearest $K_{\max} = 10$ vessels within 3 km are retained. Samples with fewer neighbors are padded to the fixed size, with padded entries identified by a binary validity mask.

Let $\mathbf{p}_0$ and $\mathbf{v}_0$ denote the target position and velocity at the anchor, and let $\mathbf{p}_j$ and $\mathbf{v}_j$ denote the corresponding state of neighbor j. The relative position and velocity are

$$\mathbf{r}_j = \mathbf{p}_j - \mathbf{p}_0, \qquad \mathbf{u}_j = \mathbf{v}_j - \mathbf{v}_0.$$

Under a constant-relative-velocity assumption, Time to Closest Point of Approach and Closest Point of Approach are computed as

$$\text{TCPA}_j = -\frac{\mathbf{r}_j^\top \mathbf{u}_j}{\|\mathbf{u}_j\|_2^2 + \varepsilon}, \qquad \text{CPA}_j = \left\|\mathbf{r}_j + \text{TCPA}_j \mathbf{u}_j\right\|_2.$$

Both quantities use only states available at the anchor. The released implementation applies the configured clipping and normalization before these attributes are supplied to a model. No state from the prediction interval is used.

The validity mask is defined as

$$m_{i,j} = \begin{cases} 1, & \text{if neighbor } j \text{ is present and valid,} \\ 0, & \text{if the entry is padded or unavailable.} \end{cases}$$

Pooling and attention operations exclude entries for which $m_{i,j} = 0$.

B.5 Weather, Sea-State, and Traffic Attributes

Each sample is matched at its anchor location and time to six ERA5 weather attributes and four ECMWF wave and sea-state attributes. The exact field names, units, and ordering are defined in the released schema. Nearest-port information and three indicators describing nearby fairways or traffic-separation schemes are derived separately from maritime and OpenStreetMap geometry.

All four AIS sources use the same matching procedure. Availability is determined at the sample level: an attribute is marked as unavailable when the requested time–location pair lies outside usable external-product coverage or fails the corresponding matching-quality check. Missing values are represented by availability masks and are not numerically imputed.

Per-source and per-attribute availability statistics are included in the released metadata. This allows model implementations to distinguish an unavailable attribute from a physically observed zero.

B.6 Environmental Spatial Support

The environmental crop is fixed at the anchor and remains unchanged throughout prediction. Because the crop is a square, a future trajectory is fully covered only when all of its positions remain within the ±5 km bounds on both local axes. Define

$$C_i = \mathbf{1}\left[\max_{1 \le t \le T_f} |x_{i,t}| \le 5\,\text{km} \ \wedge \ \max_{1 \le t \le T_f} |y_{i,t}| \le 5\,\text{km}\right].$$

A sample is fully covered when $C_i = 1$. The crop has a 5 km half-width and an anchor-to-corner distance of

$$5\sqrt{2} \approx 7.07\,\text{km}.$$

Endpoint displacement alone is therefore not an exact coverage test: a point between 5 and 7.07 km from the anchor may lie either inside or outside the square depending on its direction, and a trajectory may leave the crop before its endpoint. The indicator C_i should therefore be used for sample-level coverage analysis.

The 3 km neighboring-vessel radius serves a different purpose. It defines neighbor selection at the anchor and is not a spatial coverage boundary for the target's future trajectory.

Table 12: Horizon-wise prefix ADE (m) on the DMA Track B test set (N = 6,000) for models trained on the full 60-minute forecasting task, averaged over five seeds. ΔADE = $\text{ADE}_{\text{SDF}} - \text{ADE}_{\text{LSTM}}$, and gain denotes the relative ADE reduction over the LSTM baseline

Horizon	LSTM	LSTM + SDF	ΔADE	Gain
3 min	86.3	77.2	−9.1	10.6%
6 min	88.1	76.9	−11.2	12.7%
10 min	103.1	93.5	−9.6	9.3%
60 min	658.5	643.7	−14.8	2.2%

Table 11: Future endpoint displacement from the anchor

Track / region	Horizon (min)	Median (km)	P90 (km)
Track A / DMA	10	3.33	4.68
Track B / DMA	60	5.75	10.93
Track B / NOAA	60	8.09	11.47

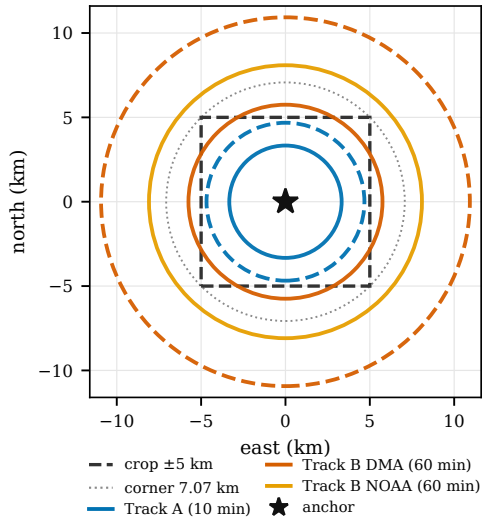


Figure 7: Fixed anchor-centered environmental crop and radial endpoint-displacement quantiles. The dashed square denotes the ±5 km crop, and the circles denote median and 90th-percentile endpoint distances. These radial summaries illustrate the greater spatial extent of Track B

C Additional Analyses and Release Details

This appendix provides additional analyses of environmental context at different prediction horizons, qualitative context examples, and a summary of the released experimental records.

C.1 Horizon-Dependent Utility of Environmental Context

Long-horizon trajectories have substantially greater spatial extent than short-horizon trajectories. Table 11 reports the displacement of the future endpoint from the anchor. For DMA, the median displacement increases from 3.33 km on Track A to 5.75 km on Track B. The corresponding Track B median for NOAA is 8.09 km.

The DMA Track A 90th-percentile endpoint displacement is below the 5 km crop half-width. In contrast, the Track B 90th percentiles for DMA and NOAA exceed the 7.07 km anchor-to-corner distance, and the NOAA Track B median also exceeds this distance (Fig. 7). These endpoint statistics illustrate the greater spatial extent of Track B but do not constitute an exact crop-coverage test. Exact sample-level coverage depends on all future positions and is defined in Appendix B.6.

To examine how environmental utility changes with the prediction horizon, we compare the SDF model with its trajectory-only LSTM backbone. Table 12 reports prefix ADE on DMA Track B over trajectories ending at 3, 6, 10, and 60 minutes, using the same five-seed protocol as the full-horizon evaluation.

The relatively large early-horizon errors of both recurrent models reflect their optimization for the complete 180-step autoregressive forecast rather than a data or metric inconsistency. Because long-range residuals are substantially larger, the full-horizon objective can trade near-term accuracy for performance over the complete rollout. Within this matched comparison, SDF conditioning reduces ADE by 9.3–12.7% over the first 10 minutes, compared with 2.2% over the full 60-minute horizon. The absolute improvement remains at 60 minutes, but its relative contribution decreases as forecasting errors accumulate. Together with the endpoint-displacement statistics, this result suggests that fixed anchor-centered context is most directly useful at earlier horizons, while its effect is diluted over long autoregressive rollouts.

This analysis does not identify limited spatial support as the sole cause of the reduced relative gain. Regional scene composition, trajectory complexity, error accumulation, and optimization variability may also contribute. The fixed crop represents a trade-off among spatial extent, resolution, storage, and computation. Multi-scale environmental representations or dynamically updated context provide possible directions for long-horizon forecasting.

C.2 Qualitative Context Examples

Figure 8 shows representative deterministic Track A predictions in different maritime scenes. The examples illustrate qualitative differences among kinematic, trajectory-only, descriptor-based, and SDF-based models and are not used for quantitative model comparison.

Figure 9 illustrates the anchor-time representation used to construct neighboring-vessel context. Positions are expressed in the target-centered local frame, and marker intensity encodes relative-speed magnitude. CPA and TCPA are computed from the same anchor-time relative positions and velocities, as defined in Appendix B.4. The presence of a nearby vessel does not by itself indicate a safety-critical encounter. The released interaction attributes are intended as forecasting context rather than as certified collision-risk estimates.

C.3 Released Experimental Records

The release includes the complete model–region result grid, intermediate-horizon metrics for both tracks, difficulty-, scene-, and neighbor-stratified evaluations, and the available per-seed records. Each result record identifies the dataset version, track,

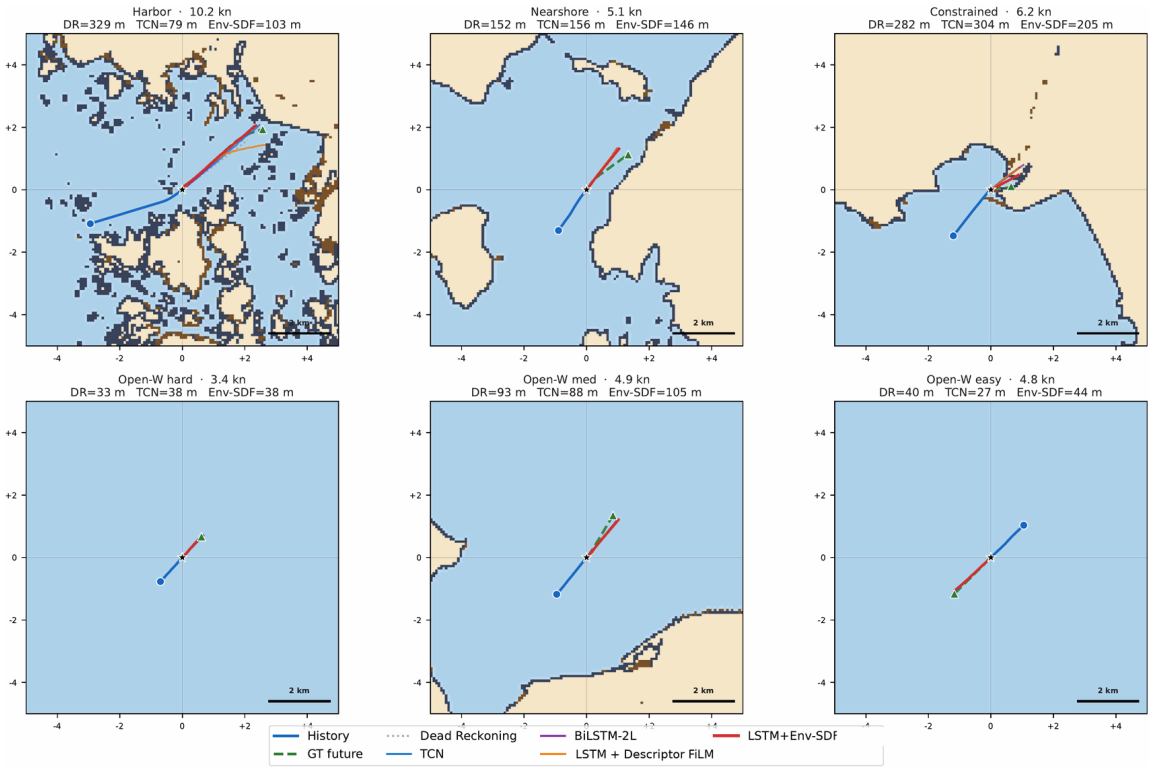


Figure 8: Representative deterministic Track A predictions across maritime scenes. Observed and ground-truth trajectories are shown together with kinematic, trajectory-only, descriptor-based, and SDF-based baselines

source region, training pool, evaluation split, temporal-consistency subset, model configuration, random seed, and selected checkpoint.

These fields distinguish experiments conducted under different source compositions, quality-control settings, and statistical protocols. The associated configuration files define model and training parameters required to reproduce each reported result.

C.4 Release, Licensing, and Intended Use

The public release contains the benchmark trajectories, sample-aligned context, quality-control metadata, construction and evaluation code, and experimental records. A stable sample identifier links each trajectory to its context records, quality flags, and split assignment without requiring additional data construction.

Because EnvShip combines multiple upstream resources, license and attribution requirements are documented separately for each source. The release includes a per-file license mapping and the corresponding attribution notices for AIS records, OpenStreetMap-derived environmental layers, and meteorological and sea-state products. Users are responsible for following the applicable upstream terms when redistributing the data or derived products.

EnvShip is intended for research on vessel trajectory forecasting, context modeling, and cross-region evaluation. The release does not add vessel ownership, operator, crew, or other identity information to the source AIS records. It should not be used to re-identify or monitor individual vessels or crews. Dataset versions, schema changes, and known issues are documented through the public release and its versioned changelog.

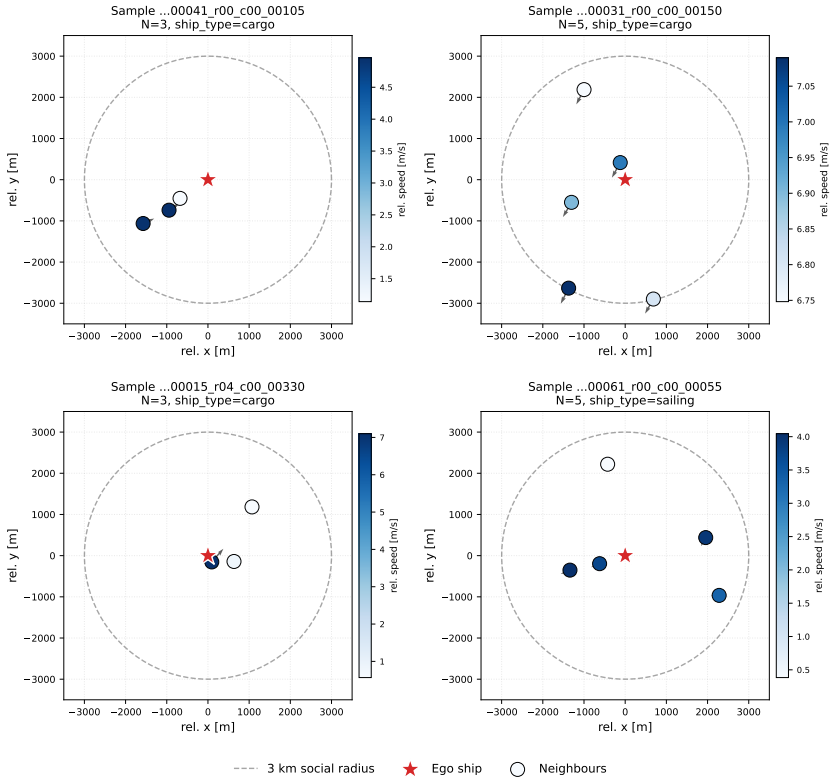


Figure 9: Neighboring-vessel context for four DMA test samples. The panels show the 3 km selection radius, target and neighboring vessels, and anchor-time relative-speed attributes